The Speed and Beam of a Ship From Its Wake's SAR Images

Gregory Zilman, Anatoli Zapolski, and Moshe Marom

***Abstract*—Synthetic aperture radar (SAR) images of ships and their wakes frequently exhibit long dark and bright streaks. Some of them can be attributed to the Kelvin wavewake and others to the turbulent and bright narrow V-wake. The wakes contain information about the ship. The present work deals with estimates of the ship beam and its velocity by processing SAR images of the Kelvin and turbulent wakes. It is assumed that the ship moves along a straight path with constant speed. For the detection of the linear features of the ship wake, the fast discrete Radon transform is employed. Once the turbulent wake is detected, the ship beam is estimated by a novel method that exploits the expansion of the turbulent wake aft a ship. A semiempirical relation between the ship beam and the width of its turbulent wake is derived and analyzed. An algorithm for estimating the width of the turbulent wake in SAR images and the ship beam is developed. The spectrum of ship-generated waves along the Kelvin cusp-lines is discussed. Processing of the lines, pertaining to the Kelvin wake bounds, and analysis of the spectral peaks enables to estimate the ship speed. Numerical examples of processing of airborne SAR images are provided.**

***Index Terms*—Radon transform, synthetic aperture radar (SAR), ship dimensions, ship wake, speed.**

I. Introduction

AIRBORNE synthetic aperture radar (SAR) images of sea surface often reveal ship wakes, which appear in the form of bright and dark streaks. Some of them pertain to the ship-generated Kelvin wavesystem and some to its turbulent wake [1], [2]. For a ship moving in deep water with constant heading angle and constant speed, the SAR images of the entire ship wake pattern are confined by two lines at an angle that is typically less than the limiting Kelvin angle of about 39° [3], [4]. The central dark streak is attributed to the ship turbulent wake. It is often bounded by two bright lines constituting the so-called narrow V-wake with a half-angle of 1.5° to 4.0° [1], [2].

SAR images of ship wakes contain specific information about the ship. The question is whether this information is sufficient for extracting certain ship characteristics, e.g., its speed and beam. Although such a question is of primary interest for ship identification by airborne SAR imaging, the number of relevant published investigations is rather limited, and the ultimate answer is unclear. This work is concerned with estimates of the ship speed and its beam by processing airborne SAR images of ship wakes.

The problem of estimating the ship particulars by analyzing its Kelvin waves (the so-called inverse ship wake problem) has been discussed by Newman [5], and later by Griffin *et al.* [6]. A point to note is that [5] deals with estimates of the ship hull cross-section parameters (not the length), whereas in [6] only the estimates of the ship length are examined. Both those methods imply that rather accurate measurements of the wave elevations within the entire wavewake are feasible. Despite the fact that interferometric synthetic aperture radars may be envisaged as a promising tool for measuring of the free-surface velocity and the wave heights [7]–[10], it is believed that in SAR images only the ship turbulent wake, narrow V-wake, and bounds of the Kelvin wave system may be distinguished. They are the most robust and reliable manifestation of the entire ship wake pattern in SAR images where the transverse and divergent Kelvin waves can be rarely seen (e.g., see [1], [2], [9], and [11], among others).

One of the most remarkable features of the far Kelvin wake is that a small boat and a supertanker moving with equal velocities might generate on the Kelvin arms waves with different amplitudes but almost of the same length. If the free surface velocity or the height of the Kelvin waves cannot be measured with sufficient accuracy, it is impossible to estimate any of the ship dimensions by processing of the Kelvin arms solely. In order to estimate at least one of the ship dimensions, i.e., its beam, we suggest to explore the properties of the ship turbulent wake.

An asymptotic relation for the expansion of the width of the turbulent wake aft a self-propelled ship with zero axial net momentum was predicted in 1957 by Birkhoff and Zarantonello [12], but only recently it has been verified for full scale vessels [13], [14]. Unfortunately, the simple formula given in [12] for the width of the turbulent wake aft a ship is purely asymptotic, i.e., it does not include any length-scale of a ship and, therefore, cannot be used for estimating the ship dimensions. Here, by invoking Birkhoff and Zarantonello hypothesis, we derive a semiempiric relation between the ship beam and the width of its turbulent wake. It depends on two empirical constants, which are evaluated by using recently obtained experimental data [13], [14]. The newly derived relation enables to estimate the ship beam. It is should be stressed that in contrast to [5] and [6], the method proposed in this work does not require any *a priori* knowledge of the ship speed.

Different methods can be used for estimating the ship speed from SAR images. In particular, the location in SAR images of the ship hull with respect to its wake provides an important information for estimating its speed (e.g., see [15]). In this paper, the speed is estimated by invoking the classic connection between the ship velocity and the kinematic features of the Kelvin wave system. Havelock [16] modeled a ship by a doublet traveling on the free surface and obtained an explicit formula relating the wave elevations and ship speed. Noting that the actual

Manuscript received September 2, 2003; revised April 5, 2004.

The authors are with the Faculty of Engineering, Tel-Aviv University, Ramat Aviv 69978, Israel (e-mail: zilman@eng.tau.ac.il).

Digital Object Identifier 10.1109/TGRS.2004.833390

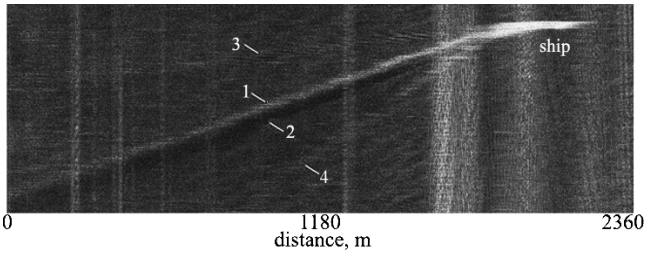

Fig. 1. SAR Image I. 1: one of the arms of the narrow V-wake; 2: turbulent wake; 3, 4: boundaries of the Kelvin wake.

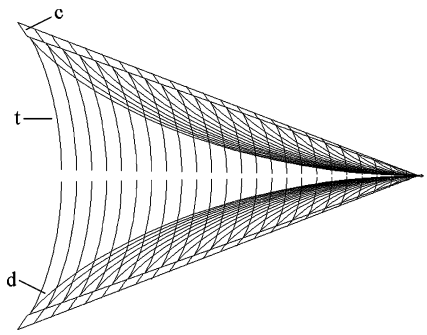

Fig. 2. Kelvin ship wake system. t: transverse, d: divergent, c: cusp waves.

ship-generated wave spectrum is continuous and narrow, Tuck *et al.* [17] proposed to estimate the ship speed by locating the sharp peaks of the wave spectra along certain cuts of the Kelvin wake (see also [18]). Here, we verify this approach by using airborne SAR images and by processing the Kelvin wake along its cusp-lines.

Processing of the turbulent wake and the boundaries of the Kelvin wake is feasible only if their location in SAR images are known. The feasibility of automatically detecting ship wakes was studied in [19]–[21]. In these works, different methods of detecting of curvilinear wakes are also proposed (see also [22]). Several authors have considered the long streaks in SAR images of the ship wakes as straight segments [19]–[25]. In line with these authors, it is assumed that the ship path is rectilinear. However, the influence of the weak curvilinearity of the ship path on the estimates is examined in the sequel.

For processing of the linear features of the ship wake, different versions of the Radon transform have been commonly employed [19]–[25]. The fast discrete Radon transform (FDRT) [26], [27] is used in the present work. FDRT speeds up our computations by a factor of 200–600, depending on the size of the SAR image.

In this paper, estimating the speed of a ship and its beam is performed by analyzing airborne ship wake images obtained by X-band SAR in experiments carried out in the eastern Mediterranean during light breeze. The ship characteristics are length $L = 52.0$ m, beam $B = 5.7$ m, speed $U = 18.0$ knots $(9.2$ m/s$)$.

A typical raw SAR image is presented in Fig. 1, where several straight segments can be clearly identified:

1) one of the two arms of the bright narrow V-wake;
2) long dark turbulent wake;
3,4) boundaries of the Kelvin wavewake.

II. Kelvin Waves and Ship Speed

The classical Kelvin wavewake consists of two different wave families, i.e., the transverse and divergent waves. If a moving ship is considered as a free-surface point disturbance, the equation of the crests of each wave system in polar coordinates (R, θ) with an origin in the disturbance can be expressed as follows [28], [29]:

$$\frac{gR_{1,2}(\theta,n)}{U^2} = \frac{4\pi[8n-\varepsilon_{1,2}]\sin\theta}{(3\mp\sqrt{1-8\tan^2\theta})^{\frac{3}{2}}(1\pm\sqrt{1-8\tan^2\theta})^{\frac{1}{2}}\cos^2\theta} \quad (n=1,2,\ldots,\varepsilon_1=1,\varepsilon_2=3) \quad (1)$$

where U is the ship speed, and g is the acceleration of gravity. The subscripts pertain to the divergent and transverse waves, respectively, and n denotes its corresponding wave crest. The entire Kelvin wavewake (Fig. 2) is bounded by two cusp-lines at an angle $\theta = 2\theta_0$, where $\theta_0 = \arctan\sqrt{1/8}$. The curves $R_n^{(1,2)}(\theta, n)$ cross the line $\theta = \theta_0$ at points having coordinates $R_{1,2}(\theta_0, n) = \pi(8n - \varepsilon_{1,2})U^2/2\sqrt{3}g$. The difference

$$\lambda_\theta = R_{1,2}(\theta_0, n+1) - R_n^{(1,2)}(\theta_0, n) = \frac{4\pi U^2}{\sqrt{3}g} \quad (2)$$

does not depend on n and, thus, defines the local wavelength on the cusp-line. Along a cusp-line, the wavenumber K_θ of the Kelvin wave and the ship speed U are related through

$$U = \sqrt{\frac{\sqrt{3}g\lambda_\theta}{4\pi}} \equiv \sqrt{\frac{\sqrt{3}g}{2K_\theta}}. \quad (3)$$

It is worthwhile to note that close to the cusp-lines the fronts of the two wave families form an angle of $55°44'$ with the ship track [28], and the wave amplitudes decay with the distance x aft the ship as $x^{-1/3}$. Inside the Kelvin angle, the decay is much faster, i.e., $x^{-1/2}$ [28].

Observation of the ship-generated waves and numerous mathematical simulations confirm that in the vicinity of the cusp-lines, wave amplitudes and wave steepness are much larger than in other parts of the wake. Possibly this may be the reason why the boundaries of the Kelvin wavewake are typically more distinguishable than the entire wave system.

It is clear from (2) that on the cusp-lines a point disturbance generates waves of the same length. For a ship of finite size, the ship-generated fluid velocity components on the free surface, as well as the corresponding wave amplitudes, can be computed within the framework of linear water wave theory and Michell thin ship approximation [30] (e.g., see [17] and [31], and more accurate approaches in [32]). An example of such a numerical simulation for a Wigley ship with parabolic waterlines is shown in Fig. 3(a). The corresponding wave spectrum along the cusp-lines shown in Fig. 3(b) is narrow, and its peak wavenumber is very close to that given by (3).

Following [19]–[25], it is assumed in this paper that the ship path is rectilinear and that the ship speed is constant. In reality, a ship may change the course or speed as a result of a turning, accelerating, or stopping maneuver. Since in open sea a ship keeps a constant average heading angle and constant speed most of the time, this situation is beyond the scope of this paper. However,

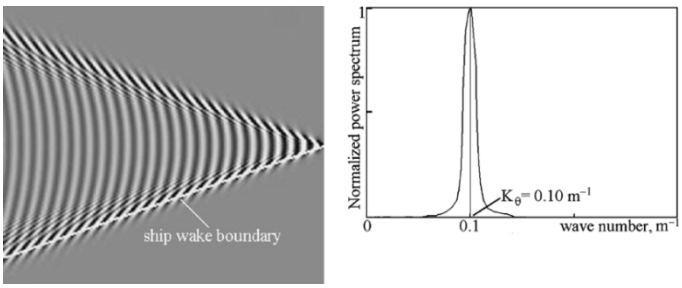

(a) (b)

Fig. 3. Longitudinal surface velocity for a ship with length $L = 52$ m, beam $B = 5.7$ m, draft $T = 3.5$ m, and speed $U = 9.2$ m/s. (a) Surface velocity component. (b) Power spectrum along the ship wake boundary. Estimate of the ship speed $\hat{U} = 9.1$ m/s.

the path of a ship may be (and in fact is) curvilinear due to unavoidable ship's yaw and sway, which depends on its inherent directional stability and weather conditions. Therefore, the effect of ship yawing is considered below.

To illustrate how yaw and sway influence the estimates of ship speed, consider first an extreme case: a ship in steady turn with turning radius r. The effect of the radius of steady turn on the kinematics of the ship wavewake was investigated in [29], [33], and [34]. In an orthogonal coordinate system Oxz with origin at the pressure point (modeling the ship), the curves of constant phase of the Kelvin waves are given by [33, p. 236, eq. 8.2.24]

$$\frac{x}{r} = \sin(\kappa\cos\gamma) - \frac{\kappa}{2}\cos^2\gamma\cos(\gamma + \kappa\cos\gamma) \tag{4}$$

$$\frac{z}{r} = 1 - \cos(\kappa\cos\gamma) - \frac{\kappa}{2}\cos^2\gamma\sin(\gamma + \kappa\cos\gamma) \tag{5}$$

where $|\gamma| < \pi/2$, $\kappa = 2\mathrm{Fr}^2\omega$, $\mathrm{Fr} = U/\sqrt{gL}$ is the Froude number, and $\omega = L/r$ is the nondimensional curvature of the path. For conventional ships, typically, the Froude number is about 0.25–0.30, whereas the normalized angular velocity ω rarely exceeds 1.0, yielding $\kappa < 0.15$–0.20. For small κ, (4) and (5) lead to the following parametric dependencies:

$$\frac{xg}{U^2} = \left[2 + (\epsilon - 1)\cos^2\gamma\right]\cos\gamma + O(\epsilon^2) \tag{6}$$

$$\frac{zg}{U^2} = (\epsilon - 1)\sin\gamma\cos^2\gamma + O(\epsilon^2) \tag{7}$$

where $|\epsilon| = \kappa|\sin\gamma| \le \kappa$. Equations (6) and (7) demonstrate that for relatively large radii of curvature, the difference in the wave lengths of the Kelvin waves on the straight course and those on a circular course $\Delta\lambda_\theta$ is of order of $\epsilon U^2/g$. It follows from (2) that the error in determining ship speed $|\Delta U/U|$ and the error in the estimate of the wavelength $|\Delta\lambda_\theta/\lambda_\theta|$ are related

$$\left|\frac{\Delta U}{U}\right| = \left|\frac{\Delta\lambda_\theta}{2\lambda_\theta}\right| = \frac{\sqrt{3}}{8\pi}\kappa \sim 0.02. \tag{8}$$

The instantaneous radius of the ship path in yaw and sway is an order of magnitude larger then in steady curvilinear motion resulting in the following error in the estimate for a yawing ship: $|\Delta U/U| \ll 1$.

III. Turbulent Wake and Ship Beam

The turbulent wake is mainly generated by turbulent skin friction of the moving ship and by propagation of hydrodynamic disturbances from the ship's boundary layer into the surrounding fluid. There is solid experimental evidence that the free-surface imbedded turbulence and surface-active materials (surfactants) typically presented in the ship turbulent wake cause a strong attenuation of short gravity-capillary waves [14]. Attenuation of the short waves leads to suppression of their spectral components, to considerable reduction in the radar back-scattering cross section, and as a consequence, to darkening of the turbulent wake in SAR images.

The width $W(x)$ of the turbulent wake of a self-propelled ship grows with large distances x aft the ship according to

$$W(x) \sim x^{\frac{1}{\alpha}} \tag{9}$$

where the predicted value of α is 5 [12].

Expression (9) is in good agreement with experimental measurements, albeit in practice α may vary between 4 and 5. Note that (9) does not include any length scale of a ship and, therefore, cannot be used for estimating the ship dimensions. One of the aims of this paper is to derive a similar formula incorporating ship beam. From dimensional analysis, the relation between the width of the turbulent wake and the beam of the ship B is of the form

$$W(x) = \left(AxB^{\alpha-1}\right)^{1/\alpha} \tag{10}$$

where the constant of proportionality A and the particular value of the constant α should be found from experiment. In this respect, we quote [14]: "The wake width subsequently grows slowly such that the half width is equal to about 2 ship beams at a distance of 4 ship lengths aft of the stern." Therefore

$$W(\bar{x}_0 L) = \bar{w}_0 B \tag{11}$$

where $\bar{x}_0 \simeq 4$ and $\bar{w}_0 \simeq 4$. Substituting (11) into (10) gives an expression for the nondimensional constant A

$$A = \frac{\bar{w}_0^\alpha}{\bar{x}_0}\frac{B}{L}$$

so that the width of the turbulent wake is

$$W(x) = \frac{\bar{w}_0}{\left(\frac{\bar{x}_0 L}{B}\right)^{1/\alpha}} B^{(\alpha-1)/\alpha} x^{1/\alpha}. \tag{12}$$

Relation (12) can be used for estimating parameters α and B as long as the width of the turbulent wake is known. The pseudo-maximum-likelihood estimator [35] based on a nonlinear transformations $\xi = \log x$ and $\tilde{W} = \log W$ yields

$$\tilde{W} = a\xi + b \tag{13}$$

where $a = 1/\alpha$ and

$$b = (1 - a)\log B + \log\frac{\bar{w}_0}{\left(\frac{\bar{x}_0 L}{B}\right)^a}. \tag{14}$$

TABLE I
WIDTH OF THE TURBULENT WAKE AFT A SHIP WITH LENGTH $L = 169.1$ m, BEAM $B = 16.75$ m MOVING WITH VELOCITY 25.0 km [13]

Distance aft the ship, x, m	0	3645	11918	21276
Width of the turbulent wake, W, m	33 ± 1	121 ± 3	145 ± 4	165 ± 5

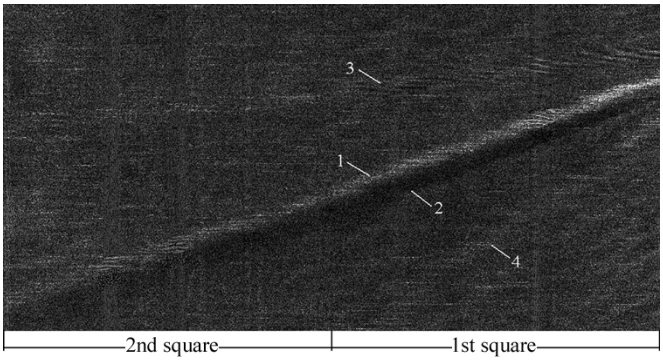

Fig. 4. $N \times 2N$ Image I. 1: one of the arms of the narrow V-wake; 2: turbulent wake; 3, 4: boundaries of the Kelvin wake.

The problem of fitting a set of given data points $\xi_i = \log x_i$ and $\tilde{W}_{ie} = \log[W(x_i)]$ $(i = 1, 2, \ldots, I)$ by adjusting a and b simultaneously can be solved by the least square method. The estimates $(\hat{\alpha}, \hat{B})$ are calculated to give

$$\hat{\alpha} = \frac{1}{a} \tag{15}$$

$$\hat{B} = \exp\left(\frac{b}{1-(1/\hat{\alpha})}\right)\left(\frac{L}{B}\right)^{1/(\hat{\alpha}-1)}\left(\frac{\bar{x}_0}{\bar{w}_0^{\hat{\alpha}}}\right)^{1/(\hat{\alpha}-1)}. \tag{16}$$

Note that in the presented approach there is no need to prescribe the parameter α in advance, since estimation of α in each particular experiment is a natural step of the algorithm. Strictly speaking, the beam B can be found from (16) only for a given ratio L/B. However, for typical values of α and ship slenderness, the function $(L/B)^{1/(\alpha-1)}$ varies rather slowly. Thus, a first guess $L/B = 10.0$ may be sufficiently accurate in practice.

The method for estimating ship beam is validated by using the results of the full-scale experiment with the width of the turbulent wake measured by several independent methods [13]. The experimental data provided in [13, Fig. 10] are digitized and presented in Table I.

Using Table I and (12)–(16) with $\bar{x}_0 = 4.0$, $\bar{w}_0 = 5.0$, and $L/B = 10.0$ results in the following estimates: $\hat{\alpha} = 5.0$, $\hat{B} = 16.6$ m and $|(B - \hat{B})/B| < 0.01$. Because of the lack of experimental information about other types of ships, the same set of parameters $\bar{x}_0$, $\bar{w}_0$, and L/B is used here.

IV. APPLICATION OF THE FAST DISCRETE RADON TRANSFORM

Consider a SAR image of $N \times N$ pixels, where $N = 2^m$, and m is an integer. Assume that the image contains straight segments approximately ten pixels wide. To detect lines with an angular resolution of, say, $\pi/M = \pi/1024$ rad in one line, the conventional Radon transform requires $N \times N \times M$ operations. In the same conditions, FDRT invokes only $N(\log_2 N)M$ operations and reduces the number of required computations by $N/\log_2 N$. The examples of airborne SAR images are of size of $1024 \times (2048$–$6144)$ pixels. Thus, for such SAR images, the speedup of the computation may be significant, by a factor of 200–600.

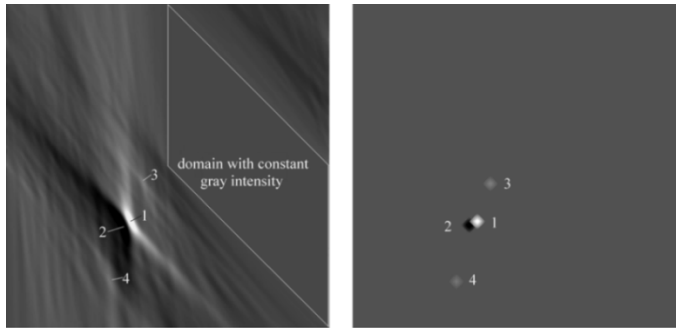

(a) (b)

Fig. 5. Radon space of the first square of Image I. (a) Raw Radon space, domain with constant gray intensity is marked. (b) Refined Radon space. The clusters 1, 2, 3, and 4 correspond to the bright and dark lines with the same numbers that in Fig. 4.

Since FDRT processes square images, an original image is divided into equal $N \times N$ squares, and FDRT is applied to each square fragment. Next, following [27], the original $N \times N$ image is transformed into $N \times 2N$ image by padding $N \times N$ artificial pixels with gray intensity corresponding to the average brightness intensity of the initial image. Then, FDRT is applied for angles of integration between zero and $\pi/4$. Finally, to cover the entire required range of angles of integration, the real image is sequentially rotated by an angle $-\pi/4$ until the entire image is processed.

In Image I (Fig. 4), the observed streaks represent the boundaries of the Kelvin wavewake, the turbulent wake, and one of the arms of the bright V-wake. The raw Radon space of the first square of the Image I is presented in Fig. 5(a), where four clusters corresponding to four intensity peaks are clearly visible: bright-1, dark-2, and pale-3, 4. The bright peak corresponds to one of the arms of the narrow V-wake; the dark extremum relates to the turbulent wake; and the pale clusters pertain to the bounding arms of the Kelvin wavewake.

The artificially padded domain results in the domain of constant gray intensity in the raw Radon image [Fig. 5(a)]. This intensity is defined as the background of the refined Radon image Fig. 5(b). A small percentage of the brightest points in cluster 1 [Fig. 5(a)] form the bright cluster 1 in Fig. 5(b). Similarly, a small percentage of the darkest points in cluster 2 [Fig. 5(a)] form the dark cluster 2 in Fig. 5(b). Once the most dark and bright streaks are detected, it is assumed that they manifest the turbulent and the bright V-wake.

To detect the pale clusters 3 and 4, a method similar to that proposed by Copeland *et al.* is used here [20]. Since the Kelvin wave pattern is well defined geometrically, clusters 3 and 4 are searched on both sides of the dark line within the limiting Kelvin angle of 39°. The standard deviation of the brightness of the raw image from the gray background σ defines the adaptive lower threshold $k_\sigma \sigma$ where $k_\sigma > 1$ is an adaptive parameter (1.2, or so). The points with brightness above this threshold form the pale clusters 3 and 4 in Fig. 5(b). If the brightness of all the processed points is below the lower adaptive threshold, the arms of

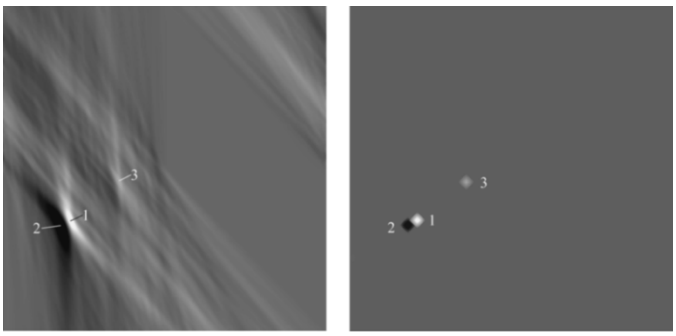

(a) (b)

Fig. 6. Radon space of the second square of Image I. (a) Raw Radon space. (b) Refined Radon space. Cluster 4 is absent according to Fig. 4.

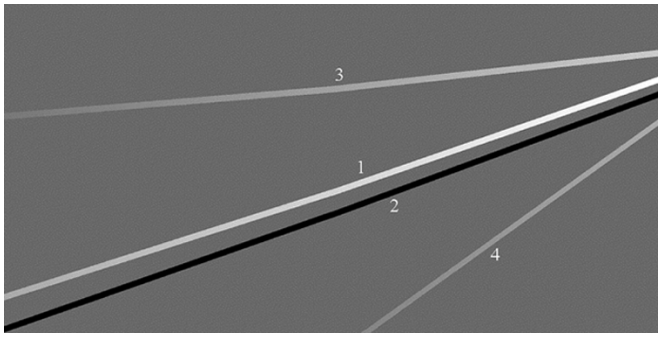

Fig. 7. Processing of Image I by the FDRT (Figs. 1 and 4).

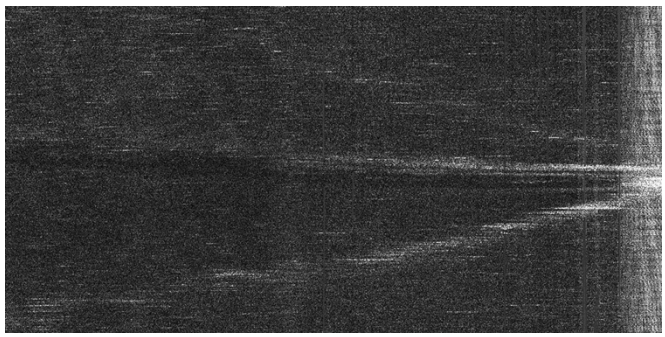

(a)

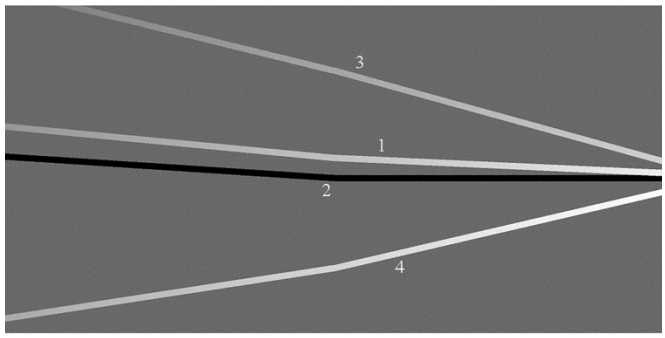

(b)

Fig. 8. Image II. (a) Raw image. (b) Results of the FDRT processing.

the Kelvin wake are not detected. Such a situation is shown in Fig. 6(a) and (b), where only one pale cluster 3 can be distinguished. In the original image, it pertains to one of the Kelvin arms of the second square, whereas the second Kelvin arm is not detected. Once the location of the clusters pertaining to the detected lines is specified, the coordinates of the points of maximum intensity inside each cluster are also known. The two coordinates of maximum intensity of each cluster in the Radon space define the endpoint of the detected line and its orientation in the original image [36].

It should be noted that the speckle noise associated with SAR images may affect the detection of the Kelvin bounds. Following [37] and [38], it is assumed here that the operation of integration, which is incorporated into the Radon transform, reduces the speckle noise and does not drastically influence the coordinates of the lines in the Radon space. This assumption is verified by comparing the location of the linear features in the SAR image and those restored from the Radon image (e.g., see Figs. 5 and 7–10). The consistency of the raw images and the detected lines is clear.

The power spectra of the pixel brightness variations calculated along the detected Kelvin bounds is used to calculate the ship speed. The coordinates of the dark and bright lines corresponding to the turbulent and V-wakes are used for determining the width of the turbulent wake aft the ship.

V. Numerical Results and Discussion

A. Ship Speed

The sequence of SAR image intensity along the detected cusp-lines with length $S_k \simeq 1$ km is used as input data for the spectral analysis. Standard periodograms obtained by fast Fourier transform are employed for this purpose. To enhance the accuracy of estimates, the spectrograms are calculated along three parallel cuts separated by a distance of order of one pixel where one of these cuts always coincides with that detected by FDRT. The resulting spectrum is obtained by averaging the three spectra and by employing the Daniell spectral estimator [39], [40].

The spectra of the ship-generated waves along the Kelvin cusp-lines involve unavoidable noise stemming from wind-generated waves and errors of measurements including speckle noise. Speckle noise can introduce physically irrelevant oscillations of pixel brightness and distort the spectra of ship waves along the Kelvin bound. It has been recently shown that speckle noise may lead to biasing of the spectral components of the calculated spectra but does not shift the frequencies of the spectral peaks as long as one is concerned with uncorrelated noise [41]. Practically, the speckle noise is correlated. However, it is assumed here that the spectra of the speckle noise is wide comparing to the ship wave spectra. In addition, to suppress irrelevant components of the calculated ship wave spectra, a preliminary eight-pole Butterworth filter with zero phase shift is employed here [40]. The parameters of the filter with bandpass $0.04 < K_\theta < 1.3\ \mathrm{m}^{-1}$ are chosen to determine correctly the maximal peak of the calculated spectra for conventional displacement ships with typical range of cruise velocities varying between 5–30 knots.

The power spectra of SAR image intensity along the cusp-lines of the Kelvin wavewake are shown in Fig. 11(a)–(c), where the sharp peaks correspond to the estimates of the wave number K_θ. The estimates of the ship speed obtained by employing (3) are given in Table II.

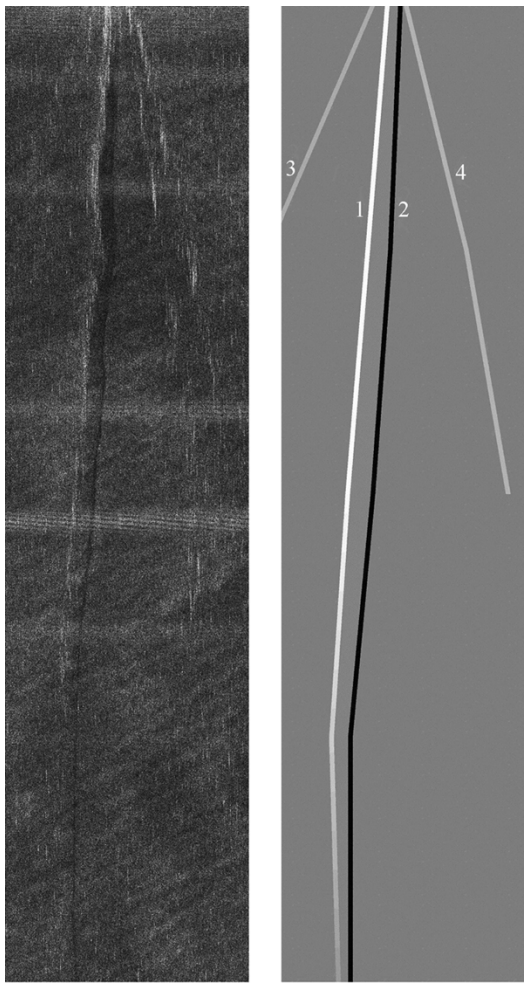

(a) (b)

Fig. 9. Image III. (a) Raw image. (b) Results of the FDRT processing.

It is seen from these examples that the discussed method gives satisfactory estimates of the real ship speed $U = 9.2$ m/s.

The obtained estimates of the ship speed may be affected by the resolution of the SAR and the length of the processed line. First, for accurate estimates of the ship speed, the SAR resolution h has to be much smaller than the wavelength $\lambda_\theta = 2\pi/K_\theta$, whereas the length of the processed line S_k has to be much larger than the wavelength. *A posteriori* verification shows that in our case the conditions $h \ll \lambda_\theta \ll S_k$ are satisfied. From (3), it follows that the error in determining ship speed $|\Delta U/U|$ and the error in the estimating the wavelength $|\Delta K_\theta/K_\theta|$ relate as

$$\left|\frac{\Delta U}{U}\right| = \left|\frac{\Delta K_\theta}{2K_\theta}\right|. \tag{17}$$

The error ΔK_θ in determining the peak wavenumber K_θ by discrete Fourier transform is equal to the spectral resolution $\Delta K = 2\pi/S_k$. Thus, the minimum length of the processed line aft the ship $S_{k\min}$ and the maximal permissible error of estimating ship speed $|\Delta U/U|_{\max}$ relate as

$$S_{k\min} \geq \frac{\pi}{K_\theta \left|\frac{\Delta U}{U}\right|_{\max}}. \tag{18}$$

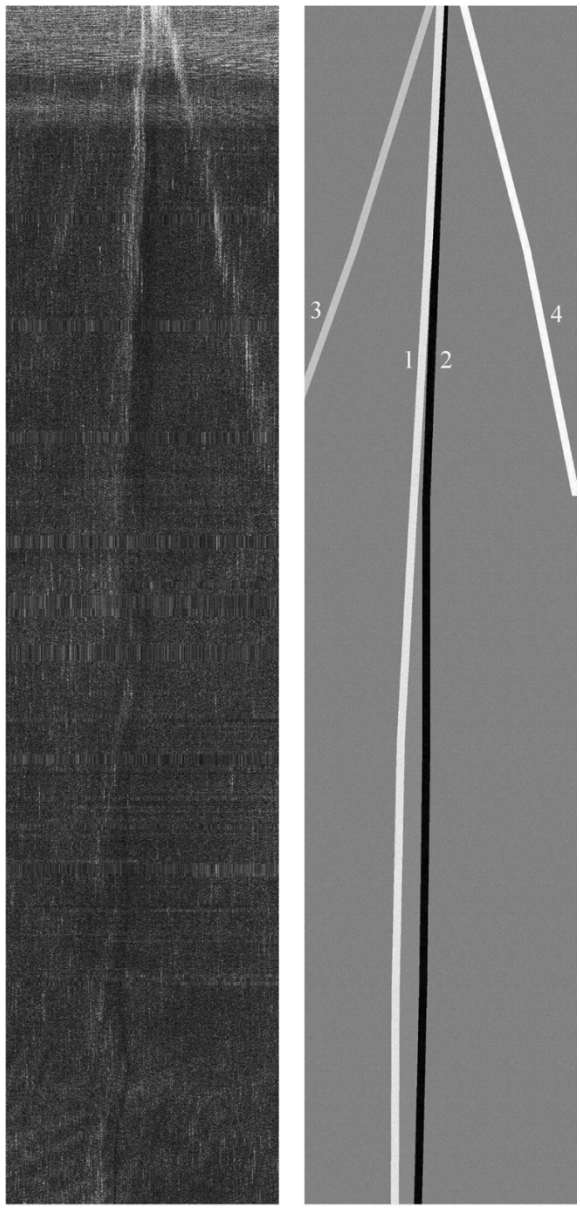

(a) (b)

Fig. 10. Image IV. (a) Raw image. (b) Results of the FDRT processing.

For instance, for estimating the ship speed in the present case $(K_\theta \simeq 0.1)$ with a relative error of about 3%, the length of the processed line aft the ship has to be of order of 1 km. This is consistent with the real length of the processed line.

B. Ship Beam

The distributions of SAR image intensity along a certain cross cut of the turbulent wake is illustrated in Fig. 12(a) exhibiting a global minimum and two maxima. One of the maxima, i.e., the bright arm of the narrow V-wake, designates the apparent bound of the turbulent wake. The distance between the brightness minimum and the brightness global maximum defines the first-guess half-width of the turbulent wake $(1/2)W$. The algorithm for calculating the total width of the turbulent wake is based on the realistic assumption that the distance between the center of the turbulent wake (the global minimum) and its second bound (the

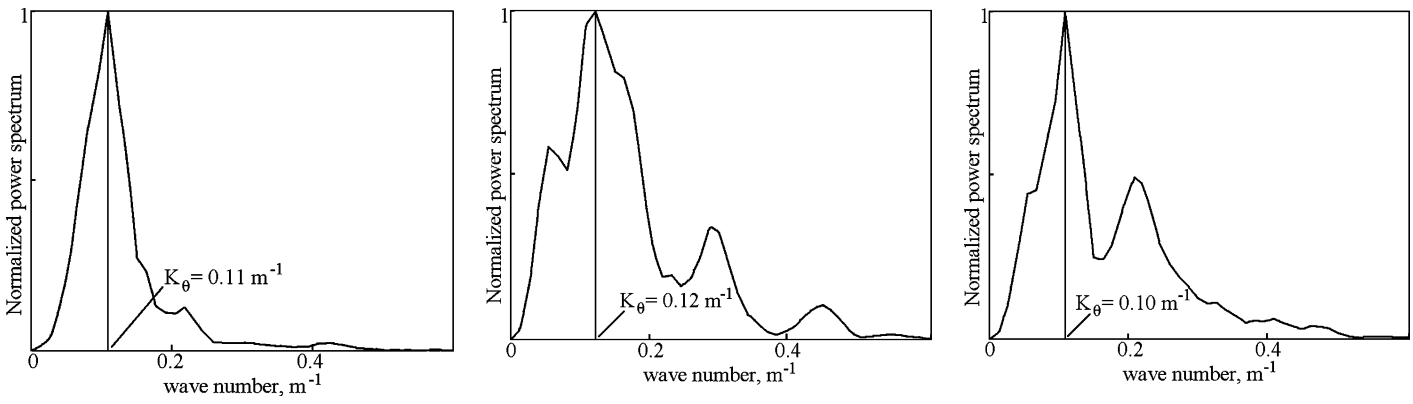

(a) (b) (c)

Fig. 11. (a) Image I (Fig. 4). Power spectrum of SAR image intensity along the Kelvin cusp-line 3. (b) Image II (Fig. 8). Power spectrum of SAR image intensity along the Kelvin cusp-line 4. (c) Image III (Fig. 9). Power spectrum of SAR image intensity along the Kelvin cusp-line 4.

TABLE II
ESTIMATES OF THE SHIP SPEED

SAR image	I	II	III
Figure	4	8	9
Estimated ship speed, $\hat{U}$, m/s	8.8	8.4	8.9
Relative error, 100($U-\hat{U}$)/U	4%	9%	3%

TABLE III
ESTIMATES OF THE SHIP BEAM

SAR image	II	III	IV
Figure	8	9	10
$\hat{\alpha}$	4.99	4.03	4.62
$\hat{B}$, m	6.3	5.5	6.0
Relative error, 100($B-\hat{B}$)/B	10%	4%	5%

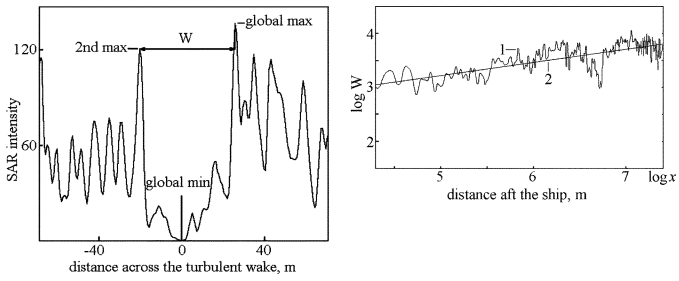

(a) (b)

Fig. 12. Image III. (a) Intensity variation in pixel brightness across the turbulent wake at distance of 1400 m aft the ship (Fig. 9). (b) Width of the turbulent wake: 1: measurements; 2: fitting by the least square method ($\alpha = 4.02, b = 1.97$).

second maximum) is always less than first-guess value W. The second maximum is searched within the indicated range. The distance between the first and second maxima is defined as the width of the turbulent wake. Certainly, such a definition of the width of the turbulent is not rigorous. It is not and need not be identical to that given by (10). However, it is adopted here, since it enables an explicit estimate of the ship beam, which may be compared against the real ship beam.

An example of the width of the turbulent wake as a function of the distance aft the ship is plotted in Fig. 12(b), where the parameters of the straight line (13) are calculated by the least square method. The results of estimation of the ship beam are presented in Table III.

It is seen from these examples that the discussed method gives satisfactory estimates of the real ship beam $B = 5.7$ m.

It should be noted that accurate extraction of maxima of the pixel brightness within the turbulent wake may be difficult. It is not clear whether the significant noise presented in Fig. 12(b) is attributed to speckle, to nonuniform distribution of surface active materials within the wake [14], to existence of large vortical structures at the oscillating boundaries of the wake, to refection of ambient waves from the turbulent wake, or to some other complex phenomena. It is not easy to determine their separate effect. To verify the robustness of the suggested method, the following mathematical simulation is carried out: for a given set of parameters (α, B) the width of the turbulent wake $W(x)$ [see (12)] is calculated and then distorted by discrete noise. The simulated values of $W(x)$ are used as input data for estimating the ship beam. The solution of the inverse problem for different types of noise allows us to evaluate the bias of the corresponding estimates ($\hat{\alpha}$, $\hat{B}$) and the relative errors $|(\alpha-\hat{\alpha})/\alpha|$ and $|(B-\hat{B})/B|$. The value of these errors may serve as an indication of the robustness of the method.

Three types of noise are considered here: an additive Gaussian noise, multiplicative uniformly distributed noise, and multiplicative Gaussian noise. The standard deviation of the noise is selected to be of the same order of magnitude that *a posteriori* standard deviation σ_W given by

$$\sigma_W = \sqrt{\frac{1}{I}\sum_{i=1}^{I}\left[W_{ie}(x_i) - W(x_i,\hat{\alpha},\hat{B})\right]^2}. \qquad (19)$$

A typical example of the distorted width of the turbulent wake is shown in Fig. 13, illustrating that the distortions are much larger than the resolution of the SAR used in our experiment. A typical example of estimates of the ship beam is provided in Table IV.

The mathematical simulation shows that for all types of noises, the bias is much less than the true value of the estimated parameter. It allows us to assert that even a relatively large local errors of evaluating the width of the turbulent wake (of order of ten meters in our case) does not influence essentially

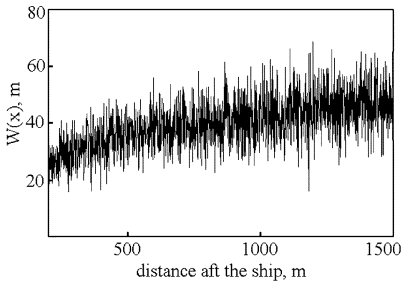

Fig. 13. Example of the width of the turbulent wake distorted by the multiplicative Gaussian noise.

TABLE IV
INFLUENCE OF NOISE ON ERRORS OF ESTIMATES ($\sigma_W = 7.2$ m)

Ship beam	True value, m	Estimate, m	Bias, m	Relative error
Additive Gaussian noise	5.7	5.9	0.2	4%
Multiplicative uniform noise	5.7	6.0	0.3	5%
Multiplicative Gaussian noise	5.7	5.9	0.2	4%

TABLE V

I. Detection of linear features in SAR images	
I−a. Calculation of the Radon transform and of the Radon image	
I−b. Processing of the Radon image to find dark and bright clusters	
I−c. Refining the Radon image by using a priory information	
I−d. Determining the angle and the location of the straight lines pertaining to the turbulent wake and Kelvin wake bounds	
II. Parallel steps	
Estimate of the ship speed	**Estimate of the ship beam**
II−a. Calculation of the spectrograms along wake bounds	*II−a.* Calculation of the width of the turbulent wake
II−b. Estimation of the ship speed	*II−b.* Estimation of the ship beam
II−c. A posteriori verification of the accuracy of estimates	*II−c. A posteriori* verification of the accuracy of estimates

the estimate of the ship beam. Nevertheless, the actual error of estimating the ship beam may be larger than those given in Table IV (see Table III, Image II). Presumably, it may be a result of a simplified hydrodynamic model, which is used here to simulate the widths of the turbulent wake. In particular, this model does not take into account the unsteady nature of the ship sway and yaw and the possible weak curvilinearity of the ship path.

The error of estimating the ship beam depends on the length of the processed dark line. The results of the above mathematical simulations show that the ship beam estimates are well behaved and do not depend essentially on the length of the processed line if it not less than 200 B. This approximate limiting value has to be verified for other types of vessels.

VI. SUMMARY OF THE ALGORITHM

The proposed algorithm of the ship identification includes the detection of ship wakes by the fast discrete Radon transform and two parallel steps shown in Table V.

VII. CONCLUSION

This paper is an attempt at solving the relatively new problem of estimating the ship beam and speed by processing SAR images of ship wakes. One contribution of this paper is a method of estimating the ship beam by processing its ship turbulent wake. A semiempirical formula relating the width of the turbulent wake and the ship beam has been obtained. A novel algorithm for estimating the ship beam has been developed and validated.

Another contribution is a validation of the ship speed estimating method by calculating the spectrum of ship-generated waves along the Kelvin wake bounds detected in real (not simulated) SAR images. For detecting the turbulent and the Kelvin wake, the fast Radon transform is applied to SAR images for the first time with high effectiveness.

The robustness of the ship beam and speed estimating methods have been tested and discussed in the case of a ship performing maneuvers with instantaneous radius of curvature much larger then the ship length.

This work is based on several assumptions that should be verified by future work. In particular, the set of empirical constants defining the width of the turbulent wake needs in further validations. The number of SAR images used is this study is still not large enough to assert with high confidence that the method is robust for various ships and weather conditions. Finally, the proposed method is not intended for processing of curvilinear and unsteady wakes. Further investigations are required in this respect.

ACKNOWLEDGMENT

The authors thank L. Shemer for his constant interest in discussing our work. They acknowledge L. Kagan for advises in numerical simulations.

REFERENCES

[1] A. M. Reed, R. F. Beck, O. M. Griffin, and R. D. Peltzer, "Hydrodynamics of remotely sensed surface ship wakes," *Trans. Soc. Nav. Arch. Marine Eng.*, vol. 99, pp. 319–363, 1990.
[2] A. M. Reed and J. H. Milgram, "Ship wakes and their radar images," *Annu. Rev. Fluid Mech.*, vol. 34, pp. 469–502, 2002.
[3] H. Lamb, *Hydrodynamics*, 6th ed. New York: Dover, 1945.
[4] J. F. Vesecky and R. H. Stewart, "The observations of ocean surface phenomena using imagery from the SEASAT synthetic aperture radar: an assessment," *J. Geophys. Res.*, vol. 87, no. C5, pp. 3397–3430, 1982.
[5] J. N. Newman, "The inverse ship-wave problem," in *Proc. 6th Int. Workshop Water Waves and Floating Bodies*, J. N. Newman, Ed., 1991, pp. 193–197.
[6] O. M. Griffin, H. T. Wang, and G. A. Meadows, "Ship hull characteristics from surface wake synthetic aperture radar (SAR) imagery," *Ocean. Eng.*, vol. 23, pp. 363–383, 1996.
[7] M. Marom, L. Shemer, and E. B. Thornton, "Energy density directional spectra of nearshore wavefield measured by interferometric synthetic aperture radar," *J. Geophys. Res.*, vol. 96, pp. 22 125–22 134, 1991.
[8] L. Shemer and E. Kit, "Simulation of an interferometric SAR imagery of an ocean system consisting of a current and a monochromatic wave," *J. Geophys. Res.*, vol. 96, pp. 22 063–22 074, 1991.
[9] L. Shemer, L. Kagan, and G. Zilman, "Simulation of ship wake image by an along-track interferometric SAR," *Int. J. Remote Sens.*, vol. 17, pp. 3577–3597, 1996.
[10] G. Zilman and L. Shemer, "An exact analytic representation of a regular or interferometric SAR image of ocean swell," *IEEE Trans. Geosc. Remote Sensing*, vol. 37, pp. 1015–1022, Mar. 1999.

[11] I. Hennings, R. Romeiser, W. Alpers, and A. Viola, "Radar imaging of Kelvin arms of ship wakes," *Int. J. Remote Sens.*, vol. 20, pp. 2519–2543, 1999.
[12] G. Birkhoff and E. H. Zarantonello, *Jets, Wakes and Cavities*. New York: Academic, 1957.
[13] R. Peltzer, J. H. Milgram, R. Skop, J. Kaiser, O. Griffin, and W. Barger, "Hydrodynamics of ship wake surfactant films," in *Proc. 18th Symp. Naval Hydrodynamics*. Washington, DC: Nat. Acad. Press, 1991, pp. 533–552.
[14] J. H. Milgram, R. A. Skop, R. D. Peltzer, and O. M. Griffin, "Modeling short sea wave energy distribution in the far wakes of ships," *J. Geophys. Res.*, vol. 98, pp. 7115–7124, 1993.
[15] J. K. Tunaley and K. E. James, "The estimation of ship velocity from SAR imagery," in *Proc. IGARSS*, vol. 1, 2003, pp. 191–193.
[16] T. T. Havelock, "The propagation of group of waves in dispersive media, with application to waves on water produced by a travelling disturbance," *Proc. R. Soc. London, Ser. A*, vol. 81, no. 549, pp. 398–430, 1908.
[17] E. O. Tuck, J. I. Collins, and W. H. Wells, "On ship patterns and their spectra," *J. Ship Res.*, vol. 15, pp. 11–21, Mar. 1971.
[18] J. D. Lyden, R. R. Hammond, D. R. Lyzenga, and R. A. Shuchman, "Synthetic aperture radar imaging of surface ship wakes," *J. Geophys. Res.*, vol. 93, pp. 12293–12 303, 1988.
[19] M. T. Rey, J. K. Tunaley, J. T. Folinsbee, P. A. Jahans, J. A. Dixon, and M. R. Vant, "Application of Radon transform techniques to wake detection in Seasat-A SAR images," *IEEE Trans. Geosci. Remote Sensing*, vol. 28, pp. 553–560, Sept. 1990.
[20] A. C. Copeland, G. Ravichandran, and M. M. Trivedi, "Localized Radon transform-based detection of ship wakes in SAR images," *IEEE Trans. Geosci. Remote Sensing*, vol. 33, pp. 35–45, Jan. 1995.
[21] K. Eldhuset, "Automatic ship and ship wake detection system for spaceborne SAR images in coastal regions," *IEEE Trans. Geosci. Remote Sensing*, vol. 34, pp. 1010–1019, July 1996.
[22] A. Hendry, J. Skingly, and A. J. Rye, "Automated linear features detection and its application to curve location in synthetic aperture radar imagery," in *Proc. IGARSS*, Edinburgh, U.K., 1988, pp. 1521–1524.
[23] J. M. Kuo and K. S. Chen, "The application of wavelets correlator for ship wake detection in SAR images," *IEEE Trans. Geosci. Remote Sensing*, vol. 41, pp. 1506–1511, June 2003.
[24] Y. Q. Jin and S. Q. Wang, "An algorithm for ship wake detection from the synthetic aperture radar images using the Radon transform and morphological image processing," *Imag. Sci. J.*, vol. 48, pp. 159–163, 2000.
[25] E. Magli and G. Olmo, "Intelligent pattern detection and compression. An application to very low bit rate transmission of ship wake aerial images," *Pattern Recognit. Lett.*, vol. 20, pp. 215–220, 1999.
[26] W. A. Götz and H. J. Druckmüller, "A fast digital Radon transform-an efficient means for evaluating the Hough transform," *Pattern Recognit.*, vol. 29, pp. 711–718, 1996.
[27] M. L. Brady, "A fast discrete approximation algorithm for the Radon transform," *SIAM J. Comput.*, vol. 27, pp. 107–119, 1998.
[28] F. Ursell, "On Kelvin ship-wave pattern," *J. Fluid Mech.*, vol. 8, pp. 418–431, 1960.
[29] L. N. Sretenskii, *The Theory of Fluid Wave Motion*. Moscow: Nauka, 1977. In Russian.
[30] A. A. Kostyukov, *The Theory of Ship Waves and Wave Resistance*. Iowa City, IA: Effective Communications, 1968.
[31] G. Zilman and T. Miloh, "Kelvin and V-like ship waves affected by surfactants," *J. Ship Res.*, vol. 45, pp. 150–163, 2001.
[32] L. J. Doctors and R. F. Beck, "Numerical aspects of the Neumann-Kelvin problem," *J. Ship Res.*, vol. 31, pp. 1–13, 1987.
[33] J. J. Stoker, *Water Waves*. New York: Wiley, 1957.
[34] E. Avital and T. Miloh, "On the determination of density profiles in stratified seas from kinematical patterns of ship-induced internal waves," *J. Ship Res.* , vol. 38, pp. 308–318, 1994.
[35] Y. Bard, *Nonlinear Parameter Estimation*. New York: Academic, 1974.
[36] R. N. Bracewell, *Two-Dimensional Imaging*. Upper Saddle River, NJ: Prentice-Hall, 1995.
[37] L. M. Murphy, "Linear features detection and enhancement in noisy images via the Radon transform," *Pattern Recognit. Lett.*, vol. 4, pp. 279–284, 1986.
[38] G. Hall, T. J. Terrell, J. M. Senior, and L. M. Murphy, "A new fast discrete Radon transform for enhancing linear features in noisy images," in *Proc. 3rd Int. Conf. Image Processing Its Applications*, London, U.K., 1989, pp. 187–191.
[39] S. L. Marple, Jr., *Digital Spectral Analysis With Applications*. Englewood Cliffs, NJ: Prentice-Hall, 1987.
[40] E. R. Kanasewich, *Time Sequence Analysis in Geophysics*. Edmonton, AB, Canada: Univ. Alberta Press, 1981.
[41] A. D. Goldfinger, "Estimation of spectra from speckled images," *IEEE Trans. Aerosp. Electron. Syst.*, vol. AES-18, pp. 675–681, 1982.

Gregory Zilman received the M.S. degree in hydrodynamics and the Ph.D. degree in naval hydrodynamics from the Leningrad (St. Petersburg) Shipbuilding Institute, Leningrad, Russia, in 1971 and 1978, respectively.

He is currently with the Department of Fluid Mechanics and Heat Transfer, Tel-Aviv University, Tel-Aviv, Israel. He is an author of a book on ship hydrodynamics and an editor of three books on marine hydrodynamics. His main research interests are marine hydrodynamics, including wave motion, ship-generated surface, and internal waves, as well as microwave remote sensing of sea surface. He was with the Leningrad (St.-Petersburg) Shipbuilding Institute for 20 years.

Dr. Zilman received the ASME Best Paper Award for his work on ship-generated internal waves in 1992. In 1993, the President of Israel presented him with the Prize of Excellence of the Ministry of Science and Technology of Israel.

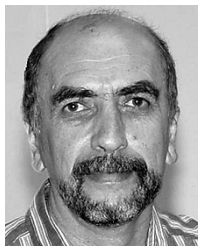

Anatoli Zapolski received the M.S. degree in electronic engineering from the Leningrad (St. Petersburg) Institute of Precise Mechanics and Optics, Leningrad, Russia, in 1974, and the Ph.D. degree in physics from the Pacific Oceanological Institute of the Russian Academy of Sciences (POI RAS), Vladivostok, Russia.

He was a Senior Researcher with POI RAS from 1985 to 1999, and was a Lecturer in physics at the Far-Eastern State Sea Academy. He is currently with the Department of Fluid Mechanics and Heat Transfer, Tel-Aviv University, Tel-Aviv, Israel. His research interests include hydro- and seismoacoustics and image and signal processing.

Moshe Marom received the B.S. and M.S. degrees in electrical engineering from the Israel Institute of Technology—Technion, Haifa, in 1979 and 1988, respectively, and the Ph.D. degree in physical oceanography from the Naval Post Graduate School, Monterey, CA, in 1990.

From 1987 to 1990, he was involved in joint projects with the National Aeronautics and Space Administration Jet Propulsion Laboratory, Pasadena, CA. He is a Consultant of a research and development company RAMOT, Ltd., at Tel-Aviv University. His research interests include SAR and INSAR imaging of ocean surface currents and wave fields.